

Prefactor in the dynamically assisted Sauter-Schwinger effect

Christian Schneider and Ralf Schützhold*

Fakultät für Physik, Universität Duisburg-Essen, Lotharstr. 1, 47057 Duisburg, Germany

(Dated: 20 October 2016)

The probability of creating an electron-positron pair out of the quantum vacuum by a strong electric field can be enhanced tremendously via an additional weaker time-dependent field. This dynamically assisted Sauter-Schwinger effect has already been studied in several works. It has been found that the enhancement mechanism depends on the shape of the weaker field. For example, a Sauter pulse $1/\cosh(\omega t)^2$ and a Gaussian profile $\exp(-\omega^2 t^2)$ exhibit significant, qualitative differences. However, so far most of the analytical studies were focused on the exponent entering the pair-creation probability. Here, we study the subleading prefactor in front of the exponential using the worldline instanton method. We find that the main features of the dynamically assisted Sauter-Schwinger effect, including the dependence on the shape of the weaker field, are basically unaffected by the prefactor. To test the validity of the instanton approximation, we compare the number of produced pairs to a numerical integration of the full Riccati equation.

PACS numbers: 12.20.-m, 11.15.Tk

I. INTRODUCTION

The Sauter-Schwinger effect is a striking phenomenon predicted by Quantum Electrodynamics (QED), that describes nonperturbative pair creation from the QED vacuum by a strong electric field [1–4]. Intuitively, one can visualize this process as an electron tunnelling from the Dirac sea to the positive continuum. So far, direct experimental verification has not been possible, due to the extremely high critical field strength $E_S = m^2 c^3 / (\hbar q) \approx 1.3 \times 10^{18}$ V/m (corresponding to an intensity of 4.6×10^{29} W/cm²) where pair production is expected for a uniform, static electric field.

An extension that can significantly lower this threshold is *dynamical assistance* [5], where an additional weak, time dependent field with the frequency scale $\hbar\omega \ll 2mc^2$ is superimposed onto a static, or slowly varying field. In [6] the impact of different pulse shapes on the dynamically assisted Sauter-Schwinger mechanism has been compared, by calculating the exponent of the pair production rate, neglecting the fluctuation prefactor.

In the following, we will apply the *worldline instanton method* [7–13] to calculate the full pair production rate in the dynamically assisted Sauter-Schwinger effect for different shapes of time dependent pulses. Section II will give a summary of the method, which is then used in section III to yield both numerical results without any further approximations and analytical estimates in certain parameter regions. In section IV we will present the numerical methods used to solve the Riccati equation which gives the exact number of produced pairs (up to numerical accuracy).

We will work in 1+1 spacetime dimensions throughout, a choice that will be explained in section IV.

This is sufficient to represent the fields considered in this work, as we only need one spatial dimension (in

which the electric field is oriented) and the temporal dimension (to study time dependent fields) [14].

II. WORLDLINE INSTANTON METHOD

Let us first briefly review the worldline instanton method (for a detailed derivation see, e.g. [11, 12]), and in particular how the prefactor differs in 1 + 1 and 3 + 1 spacetime dimensions.

We start out with the vacuum persistence amplitude, i.e., the probability amplitude that an initial vacuum state $|0_{\text{in}}\rangle$ remains vacuum $|0_{\text{out}}\rangle$, which can be expressed using the effective action Γ_M ,

$$\langle 0_{\text{out}} | 0_{\text{in}} \rangle = e^{i\Gamma_M}. \quad (1)$$

We use the subscript M to indicate Minkowskian quantities, in contrast to the Euclidean versions we will mostly be concerned with in the following.

If the effective action were to gain an imaginary part, the absolute value of the vacuum persistence would deviate from one, which can be interpreted as the probability amplitude for pair production:

$$P_{e^+e^-} = 1 - |\langle 0_{\text{out}} | 0_{\text{in}} \rangle|^2 \approx 2\Im\Gamma_M. \quad (2)$$

After analytic continuation, the Euclidean effective action can be expressed using the *worldline path integral*

$$\Gamma[A_\mu] = \int_0^\infty \frac{dT}{T} e^{-m^2 T} \int_{x(T)=x(0)=x^{(0)}} d^2 x^{(0)} \int_{x(T)=x(0)=x^{(0)}} \mathcal{D}x \times \exp \left[- \int_0^T d\tau \left(\frac{\dot{x}^2}{4} + iqA \cdot \dot{x} \right) \right] \quad (3)$$

over closed loops $x_\mu(\tau)$ in Euclidean spacetime, where μ only takes on the values 1 and 2, so $\dot{x}^2 = \dot{x}_1^2 + \dot{x}_2^2$ and $A \cdot \dot{x} = A_1 \dot{x}_1 + A_2 \dot{x}_2$. In this case x_1 denotes the spatial component (e.g. z) and x_2 imaginary time.

* ralf.schuetzhold@uni-due.de

Note that we are considering *scalar* QED here, i.e. a complex scalar field coupled to the electromagnetic potential. Compared to QED this lacks the spin degree of freedom, which for the class of fields studied in the following can be shown to result in a trivial factor of 2 only [11].

The worldline instanton approach is a semiclassical approximation to (3), by evaluating both the path integral and the integral over T using the saddle point method.

For the path integral, we need to find a path $x_\mu(\tau)$ with $x_\mu(T) = x_\mu(0)$ that extremizes

$$\mathcal{A}[x_\mu](T) = \int_0^T d\tau \left(\frac{\dot{x}^2}{4} + iqA \cdot \dot{x} \right) \quad (4)$$

for a given T . The Euler-Lagrange equations for this action functional give the equations of motion

$$\ddot{x}_\mu = iqF_{\mu\nu}\dot{x}_\nu. \quad (5)$$

A solution to (5) that satisfies the periodicity conditions is called a *world line instanton*, in analogy to the instantons in nonrelativistic quantum tunneling [15].

The saddle point approximation includes an additional prefactor, arising from the fluctuations around the extremum. For the path integral, this amounts to the determinant of a second order differential operator [16]. Remarkably, this determinant can be found using a finite determinant comprised of solutions to a certain initial value problem (for a derivation using methods of complex analysis, see [17]).

Including the fluctuation prefactor, the saddle point approximation of the path integral in (3) is given by

$$\int_{x(T)=x(0)=x^{(0)}} \mathcal{D}x \exp \left[- \int_0^T d\tau \left(\frac{\dot{x}^2}{4} + iqA \cdot \dot{x} \right) \right] \\ \approx \frac{e^{i\theta}}{4\pi T} \sqrt{\frac{|\det[\eta_{\mu,\text{free}}^{(\nu)}(T)]|}{|\det[\eta_\mu^{(\nu)}(T)]|}} \exp(-\mathcal{A}[x_\mu^{\text{cl}}](T)). \quad (6)$$

The η_μ are solutions to the fluctuation equations of motion and θ is the Morse index [18] of the fluctuation operator (omitted here for brevity). In contrast to the (3+1)-dimensional case, the finite determinants are 2×2 and we get a factor of $(4\pi T)^{-1}$ instead of $(4\pi T)^{-2}$.

Let us now restrict ourselves to time dependent, homogeneous electric fields of constant direction. In particular, we use the Euclidean four-potential

$$iA_1 = \frac{E}{\omega} f(\omega x_2), \quad (7)$$

leading to the electric field

$$\mathbf{E} = E f'(i\omega t) \mathbf{e}_z. \quad (8)$$

In this case, both the instanton action and the fluctuation determinant can be found, up to quadrature, in terms of the function f .

The remaining T -integral can be done explicitly using the saddle point approximation as well. The imaginary part of the Minkowski effective action is then completely determined by the single function

$$g(\gamma) = \frac{4}{\pi} \int_0^{\chi^*} d\chi \sqrt{1 - \frac{1}{\gamma^2} f(\gamma\chi)^2}, \quad (9)$$

where $\gamma = m\omega/(qE)$ is the *Keldysh parameter* and the turning point χ^* is determined by the implicit equation

$$\gamma = f(\gamma\chi^*). \quad (10)$$

Using this function, we find our final expression for the imaginary part of the effective action, and thus the pair production rate:

$$\Im\Gamma_{\text{M}}[A_\mu] \approx \frac{\mathcal{L}}{m^{-1}} \sqrt{\frac{E}{E_S}} \frac{\sqrt{2}}{8\pi\gamma\Phi(\gamma)} \exp\left(-\pi \frac{E_S}{E} g(\gamma)\right), \quad (11)$$

with the function

$$\Phi(\gamma) = \sqrt{-\frac{d^2}{d(\gamma^2)^2} (\gamma^2 g(\gamma))}. \quad (12)$$

The length \mathcal{L} is given by the spatial extent of the electric field, for example the focal spot of a laser beam.

To check the validity of the semiclassical approximation, we turn to a single Sauter pulse, where an exact treatment is possible. In this case (for details see [12])

$$g(\gamma) = \frac{2}{1 + \sqrt{1 + \gamma^2}}, \quad (13)$$

$$\Phi(\gamma) = \frac{1}{\sqrt{2}} (1 + \gamma^2)^{-3/4}, \quad (14)$$

and thus

$$\Im\Gamma_{\text{M}} \approx \frac{\mathcal{L}}{m^{-1}} \frac{1}{4\pi} \sqrt{\frac{E}{E_S}} \frac{(1 + \gamma^2)^{3/4}}{\gamma} \\ \times \exp\left(-\frac{E_S}{E} \frac{2}{1 + \sqrt{1 + \gamma^2}}\right). \quad (15)$$

In Fig. 1 we compare (15) to the known exact solution (see, e.g., [19]). As expected, the semiclassical approximation breaks down for large E/E_S , but even for $E = E_S/5$ the agreement is excellent, only for $E = E_S/3$ the results start to deviate visibly.

In 3 + 1 space-time dimensions, the prefactor differs from (11) by additional factors [12]

$$\frac{\Im\Gamma_{\text{M}}^{3+1}}{\Im\Gamma_{\text{M}}^{1+1}} = \frac{V_2}{m^{-2}} \frac{E}{E_S} \frac{1}{4\pi^2 \frac{d}{d(\gamma^2)} (\gamma^2 g(\gamma))}. \quad (16)$$

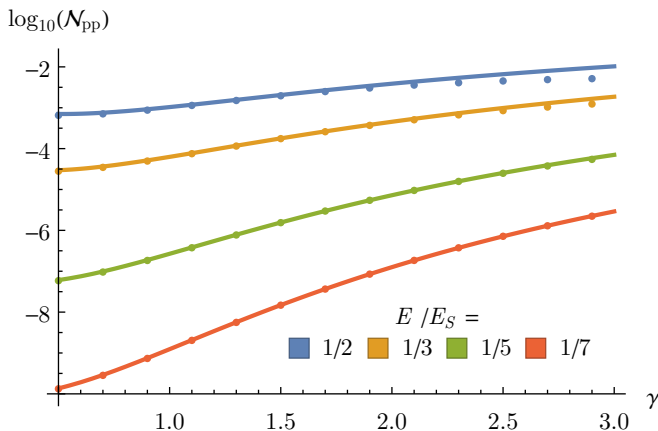


FIG. 1. Predicted number density of produced pairs by a single Sauter pulse with Keldysh parameter γ . The points depict the worldline instanton approximation (15), the lines show the exact analytical result. The field strength increases from bottom to top.

Apart from the obvious two-volume/area V_2 and an additional power of E , this also includes nontrivial scaling with γ . For the single Sauter pulse, this amounts to

$$\frac{1}{\frac{d}{d(\gamma^2)}(\gamma^2 g(\gamma))} = \sqrt{1 + \gamma^2}, \quad (17)$$

which does not modify the qualitative behavior.

III. DYNAMICALLY ASSISTED SAUTER-SCHWINGER EFFECT

We now apply (9) and (11) to the dynamically assisted Sauter-Schwinger effect.

We choose the function

$$f(\chi) = \frac{1}{\rho} \tan(\rho\chi) + \varepsilon h(\chi), \quad \varepsilon \ll 1, \quad \rho \ll 1, \quad (18)$$

representing the sum of a strong, slow field and a weak, faster profile with $E_{\text{weak}}/E = \varepsilon$, $\Omega/\omega = \rho$,

$$\mathbf{E} = E(\cosh^{-2}(\Omega t) + \varepsilon h'(i\omega t))\mathbf{e}_z. \quad (19)$$

Note that in this case, the *combined* Keldysh parameter $\gamma = m\omega/(qE)$ compares the frequency scale ω of the weak pulse with the field strength E of the slow, strong field. Note that we do not approximate the slow field by a static one (as in [6]), as the electric field has to vanish for large times for the numerical integration of the Riccati equation to work and the limit $\varepsilon \rightarrow 0$ would pose problems in the instanton method.

In the following, we will choose the following profiles for the fast pulses, see also [6]

- Cosine $\cos(\omega t)$, $h^{\text{cos}}(\chi) = \sinh \chi$
- Gaussian $\exp(-\omega^2 t^2)$, $h^{\text{Gauss}}(\chi) = \frac{\sqrt{\pi}}{2} \text{erfi } \chi$

- Sauter $\cosh^{-2}(\omega t)$, $h^{\text{Sauter}}(\chi) = \tan \chi$
- Lorentzian $(1 + \omega^2 t^2)^{-1}$, $h^{\text{Lorentz}}(\chi) = \text{artanh } \chi$

First, we will numerically calculate $g(\gamma)$ and $\Phi(\gamma)$ (and thus $\Im\Gamma_M$) for these pulse shapes $h(\chi)$. In section III B we will then present analytical approximations for the pair production rate.

A. Numerical evaluation

The effective action (11) can be evaluated straightforwardly using numerical methods. The only challenge is solving the implicit equation (10). For the cosine and Gaussian profiles, h is smooth and a simple root finding algorithm converges using basically any choice of starting point. For the other two profiles however, h diverges (at $\chi = \pi/2$ or $\chi = 1$ respectively), so for small ε , the starting points for the root finding method have to be chosen with some care.

As soon as χ^* is found, a standard numerical integration routine can be used to evaluate (9) and (12), yielding the effective action (11).

Figure 2 shows the results of this procedure. In all cases there is a region of relatively weak dependence on the frequency of the weak field and a region of strong enhancement, as soon as the Keldysh parameter crosses a threshold value γ^{crit} . For the cosine and Gauss profiles, this threshold depends on ε , while it is approximately constant for the Sauter and Lorentz pulses. This is the same behavior as seen in [6] considering the exponent only, so we can now conclude that the prefactor does not change this qualitatively.

Now that we have an approximation for the full pair production rate using the worldline instanton method, the question that remains is if this approximation actually works well for these field configurations. Thus we compare it to a solution of the full Riccati equation as outlined in section IV. In Fig. 3, we can see that both methods agree perfectly below threshold or for large ε . Only for small ε and large γ the results deviate visibly. This is very interesting, because naïvely one might expect the quality of the approximation to depend mainly on the pair production probability (as it appears to do in Fig. 1), while in this case the interplay between multiple scales leads to a different behavior.

Furthermore, for small ε the instanton method predicts a highly unintuitive “dip” just below the critical value of γ where the pair production actually decreases with increasing Keldysh parameter (visible in Fig. 3 at the lower left edge of the displayed surfaces, more obvious in Fig. 4). The numerical solution of the Riccati equation however does not show this anomaly, so we can conclude it to be an artifact of the semiclassical approximation, again stressing that its validity has to be carefully examined in each situation.

Regardless, the Riccati equation predicts the same

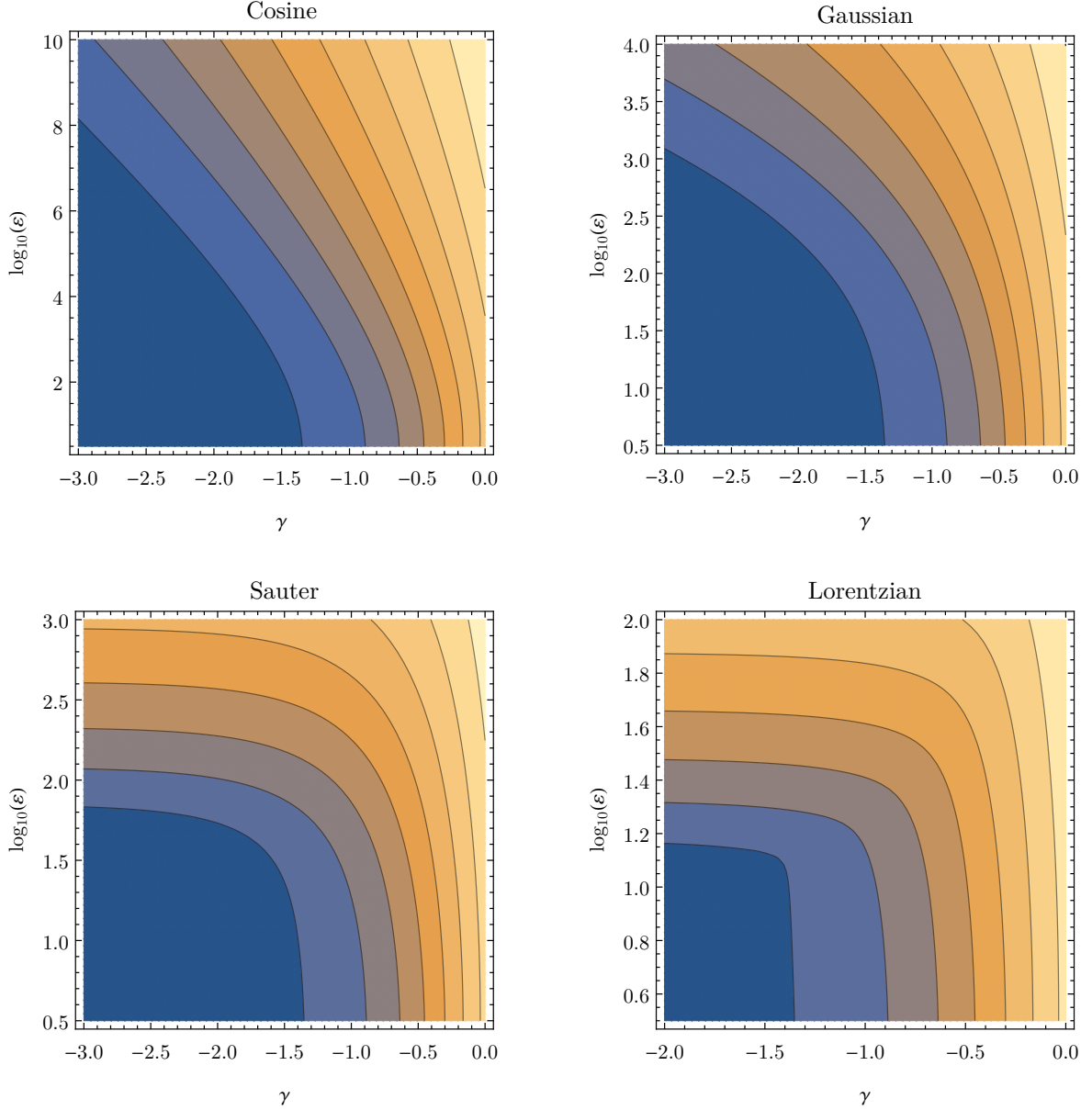


FIG. 2. Imaginary part of the effective action (11) in the assisted Sauter Schwinger effect for different pulse shapes $h(\chi)$, Keldysh parameters γ and relative field strengths ε . The color scale spans from 10^{-40} (blue, bottom left corners) to 10^{-16} (yellow, top right corners). Note the dependence of the threshold γ^{crit} on ε for the cosine and Gauss profiles, while $\gamma^{\text{crit}} \approx \text{const.}$ for the Sauter and Lorentz profiles.

qualitative result of dynamical assistance above a threshold value of γ , which is roughly independent of ε .

B. Analytical approximations

To find analytical expressions for $g(\gamma)$ and thus $\Phi(\gamma)$ and $\Im\Gamma_M$, we can use different approaches for $\gamma < \gamma^{\text{crit}}$ and $\gamma > \gamma^{\text{crit}}$.

Below threshold, we can Taylor expand $g(\gamma)$ in ε and

$$\begin{aligned}
 g(\gamma) &= \frac{4}{\pi} \int_0^{\chi^*} d\chi \sqrt{1 - \left(\frac{\tan(\rho\gamma\chi)}{\rho\gamma} + \varepsilon \frac{h(\gamma\chi)}{\gamma} \right)^2} \\
 &\approx \frac{4}{\pi} \left(\int_0^{\chi_{\varepsilon=0}^*} d\chi \sqrt{1 - \left(\frac{\tan(\rho\gamma\chi)}{\rho\gamma} \right)^2} \right. \\
 &\quad \left. - \varepsilon \int_0^1 \frac{d\chi \chi}{\sqrt{1-\chi^2}} \frac{h(\gamma\chi)}{\gamma} \right) \\
 &= \frac{2}{1 + \sqrt{1 + \rho^2\gamma^2}} - \frac{4\varepsilon}{\pi\gamma} \int_0^1 d\xi h(\gamma\sqrt{1-\xi^2}) \\
 &= \frac{2}{1 + \sqrt{1 + \rho^2\gamma^2}} - \frac{4\varepsilon}{\pi\gamma} G(\gamma). \tag{20}
 \end{aligned}$$

Note that this approximation works only for subcritical γ , because otherwise $h(\gamma\chi)$ grows large, invalidating the expansion. The ε -independent term is just the result for a single Sauter pulse with Keldysh parameter $\rho\gamma$ (see (13)).

Substituting this expression for $g(\gamma)$ in (12) we get

$$\Phi(\gamma) \approx \sqrt{\frac{\rho^2}{2(1+\rho^2\gamma^2)^{3/2}} + \frac{\varepsilon}{\pi\gamma^3}(\gamma^2 G'' + \gamma G' - G)}. \quad (21)$$

Here, it is evident why we kept the slow pulse explicit, instead of approximating it as static. If the strong field were independent of time, we would have $\Phi \rightarrow 0$ as $\varepsilon \rightarrow 0$, leading to $\Im\Gamma_M \rightarrow \infty$. This is expected, because then for $\varepsilon \rightarrow 0$, the instanton is not confined in the time direction anymore, giving rise to a zero mode. Using a slow Sauter pulse for the strong field solves this problem.

Now all that is left is to calculate $G(\gamma)$ for the different pulse profiles:

Cosine:

$$G^{\text{cos}}(\gamma) = \frac{\pi}{2} I_1(\gamma) \quad (22)$$

$$\Phi^{\text{cos}}(\gamma) = \sqrt{\frac{\rho^2}{2(1+\rho^2\gamma^2)^{3/2}} + \frac{\varepsilon I_1(\gamma)}{2\gamma}} \quad (23)$$

where I_ν denotes the modified Bessel functions of the first kind.

Gauss:

$$G^{\text{Gauss}}(\gamma) = \frac{\pi\gamma}{4} e^{\gamma^2/2} (I_0(\gamma^2/2) - I_1(\gamma^2/2)) \quad (24)$$

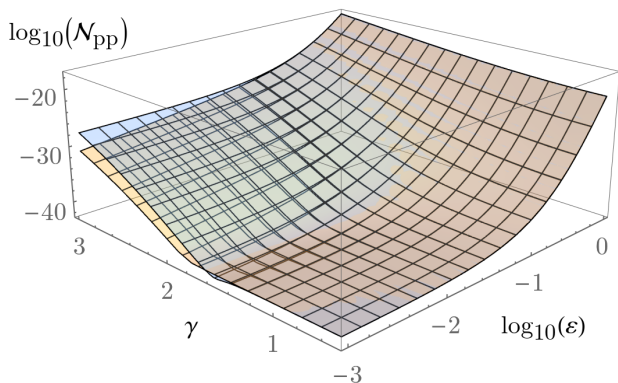


FIG. 3. Density of produced pairs from a strong, slow and another weak, fast Sauter pulse. The strong field strength is $E/E_S = 0.033$, corresponding to an intensity of $\approx 5 \times 10^{26}$ W/cm². The blue surface (lying above for large γ and small ε) is the instanton result (11), the orange surface shows the numerical integration of the full Riccati equation.

$$\Phi^{\text{Gauss}}(\gamma) = \sqrt{\frac{\rho^2}{2(1+\rho^2\gamma^2)^{3/2}} + \frac{\varepsilon}{2} e^{\gamma^2/2} \left(I_0\left(\frac{\gamma^2}{2}\right) + I_1\left(\frac{\gamma^2}{2}\right) \right)} \quad (25)$$

Lorentz:

$$G^{\text{Lorentz}}(\gamma) = \frac{\pi}{2} \frac{1 - \sqrt{1 - \gamma^2}}{\gamma} \quad (26)$$

$$\Phi^{\text{Lorentz}}(\gamma) = \sqrt{\frac{\rho^2}{2(1+\rho^2\gamma^2)^{3/2}} + \frac{\varepsilon}{2} \frac{1}{(1-\gamma^2)^{3/2}}} \quad (27)$$

For the Sauter profile, it is unfortunately not possible to find a closed form expression for the integral in $G(\gamma)$, so we can not give an analytic expression for its subcritical behavior.

For $\gamma > \gamma^{\text{crit}}$ however, the function $g(\gamma)$ can be approximated in the limit $\varepsilon \ll 1$ for the Sauter and Lorentzian pulses by geometric considerations [5, 20], leading to

$$g^{\text{Sauter}}(\gamma > \pi/2) = \frac{2}{\pi} \arcsin\left(\frac{\pi}{2\gamma}\right) + \frac{\sqrt{\gamma^2 - \left(\frac{\pi}{2}\right)^2}}{\gamma^2}. \quad (28)$$

The same method applies to the Lorentzian pulse, the only difference being the different value of the critical Keldysh parameter:

$$g^{\text{Lorentz}}(\gamma > 1) = \frac{2}{\pi} \left(\arcsin\left(\frac{1}{\gamma}\right) + \frac{\sqrt{\gamma^2 - 1}}{\gamma^2} \right). \quad (29)$$

Figure 4 shows the numerical calculation of $\Im\Gamma^{\text{Lorentz}}$ for different values of ε , the approximations (26) and (27) for $\gamma < 1$ and (29) for $\gamma > 1$. Far above threshold, the pair production rate converges to the approximation (29), independent of ε . Closer to the threshold, the geometric approach breaks down for larger values of ε , although for $\varepsilon = 10^{-2}$ the numerical values agree with the approximation very well. As expected, the approximation (26) below threshold works better, the smaller the expansion parameter ε gets.

For $\varepsilon = 10^{-2}$ the instanton method again predicts the anomalous decrease in pair production at $\gamma \approx \gamma^{\text{crit}}$ mentioned before.

IV. NUMERICAL SOLUTION OF THE RICCATI EQUATION

To test the instanton approximations we compared the results to a numerical evaluation of the Riccati equation, this chapter explains how we obtained these results. A brief derivation of the Riccati formalism can be found in [6] or in some more detail in [21]. For a time dependent field pointing in the z -direction represented by a

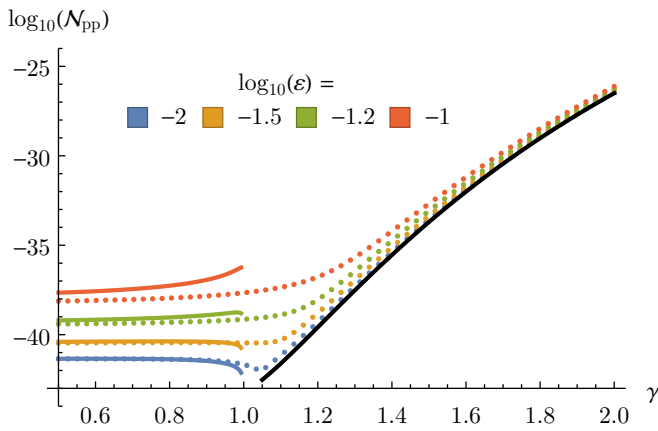


FIG. 4. Number density of produced pairs for a Lorentzian pulse. The dots represent the numerical results for different values of ε , the lines represent the approximations (26) and (27) for $\gamma < 1$ and (29) for $\gamma > 1$. ε increases from bottom to top.

vector potential $A_3(t)$, we may employ a Fourier transformation in order to account for the spatial dependence of our mode functions. After that, the time-dependence of the instantaneous Bogoliubov coefficients $\alpha_{\mathbf{k}}$ and $\beta_{\mathbf{k}}$ is governed by the Riccati equation

$$\dot{R}_{\mathbf{k}} = \Xi_{\mathbf{k}}(t) \left(e^{+2i\phi_{\mathbf{k}}(t)} + R_{\mathbf{k}}^2(t)e^{-2i\phi_{\mathbf{k}}(t)} \right) \quad (30)$$

with $R_{\mathbf{k}} = \beta_{\mathbf{k}}/\alpha_{\mathbf{k}}$ and

$$\begin{aligned} \Xi_{\mathbf{k}}(t) &= \frac{q\dot{A}_3(t)\sqrt{m^2 + \mathbf{k}_{\perp}^2}}{2\Omega_{\mathbf{k}}(t)^2}, \quad \phi_{\mathbf{k}}(t) = \int_{-\infty}^t dt' \Omega_{\mathbf{k}}(t'), \\ \Omega_{\mathbf{k}}(t) &= \sqrt{m^2 + \mathbf{k}_{\perp}^2 + (k_3 + qA_3(t))^2}, \end{aligned} \quad (31)$$

and the initial condition $R_{\mathbf{k}}(-\infty) = 0$.

Here, \mathbf{k} labels the different momentum modes, where k_3 denotes momentum parallel to the electric field and $\mathbf{k}_{\perp} = (k_1, k_2)^{\top}$ the perpendicular momenta. To arrive at the number of produced pairs per volume, we need to integrate over all modes:

$$\mathcal{N}_{\text{pp}} = \int \frac{d^3k}{(2\pi)^3} |R_{\mathbf{k}}(\infty)|^2, \quad (32)$$

where the factor of $(2\pi)^{-3}$ stems from the choice of normalization in the mode decomposition.

We will, as mentioned in the introduction, work in 1+1 spacetime dimensions, which amounts to setting $\mathbf{k}_{\perp} = 0$. This is due to the fact that we need to find $R_{\mathbf{k}}(\infty)$ for sufficiently many values of \mathbf{k} to approximate the integral in (32), which is computationally intensive. The payoff however is small: While the longitudinal momentum spectrum includes important physical effects like interference patterns (see, e.g. [21, 22]), the perpendicular momenta only amount to a rescaling of the electron mass,

as is evident in (31). This leads to further exponential suppression for $\mathbf{k}_{\perp}^2 > 0$ so they hardly contribute to (32) and especially do not modify the qualitative response of the pair production rate to the field profile.

To numerically integrate (30), we need to introduce dimensionless quantities. First, we choose the vector potential to be

$$A_3(t) = \frac{E}{\omega} f(\omega t), \quad (33)$$

with a dimensionless shape function f and scaling frequency ω . We then introduce the quantities

$$p = \frac{k_3}{m}, \quad \gamma = \frac{m\omega}{qE}, \quad \tau = \frac{tqE}{m}, \quad \mathcal{E} = \frac{E}{E_S} = \frac{qE}{m^2}, \quad (34)$$

leading to the dimensionless Riccati equation, which can be treated numerically:

$$\begin{aligned} \dot{R}_p(\tau) &= \frac{\mathcal{E}f'(\gamma\tau)}{2\left(1 + (p + f(\gamma\tau)/\gamma)^2\right)} \\ &\quad \times \left(e^{i2\varphi_p(\tau)/\mathcal{E}} + R_p^2(\tau)e^{-i2\varphi_p(\tau)/\mathcal{E}} \right), \end{aligned} \quad (35a)$$

$$\dot{\varphi}_p(\tau) = \sqrt{1 + (p + f(\gamma\tau)/\gamma)^2}. \quad (35b)$$

While $\varphi_p(\tau)$ can of course be obtained immediately in terms of an integral, this can usually not be done analytically. Now, since we would like to use a variable step width integration algorithm to solve (35), we do not know in advance for which values of τ we need $\varphi_p(\tau)$, so we cannot efficiently precompute the integral. Thus, it is most convenient to directly solve the system of equations (35) in lockstep.

Of course, we cannot perform infinitely many integration steps to find $R(\infty)$ from $R(-\infty) = 0$, but have to choose a sufficiently long time range $\tau \in [-\mathcal{T}, \mathcal{T}]$, so that $E(|\tau| > \mathcal{T})$ is negligible compared to $E(|\tau| < \mathcal{T})$. Then, using the initial condition $R_p(-\mathcal{T}) = 0$, $\varphi_p(-\mathcal{T}) = 0$ we arrive at the number of produced pairs per Compton length

$$\mathcal{N}_{\text{pp}} = \frac{1}{m^{-1}} \int \frac{dp}{2\pi} |R_p(\mathcal{T})|^2. \quad (36)$$

Unfortunately, actually obtaining $R_p(\mathcal{T})$ for large \mathcal{T} and small values of \mathcal{E} is far from trivial. Since the exponentials in the Riccati equation oscillate wildly with a frequency of order \mathcal{E}^{-1} , the step width $\Delta\tau$ has to be sufficiently small, which means many steps have to be taken to reach \mathcal{T} . Using a standard ODE integration algorithm [23], for fields weaker than $\approx E_S/10$ machine precision is not sufficient anymore and rounding errors begin to dominate.

Instead, we use the software package TIDES [24] which is based on the Taylor series method and supports the GNU MPFR [25] library for multiple precision arithmetic, allowing us to integrate the Riccati equation using

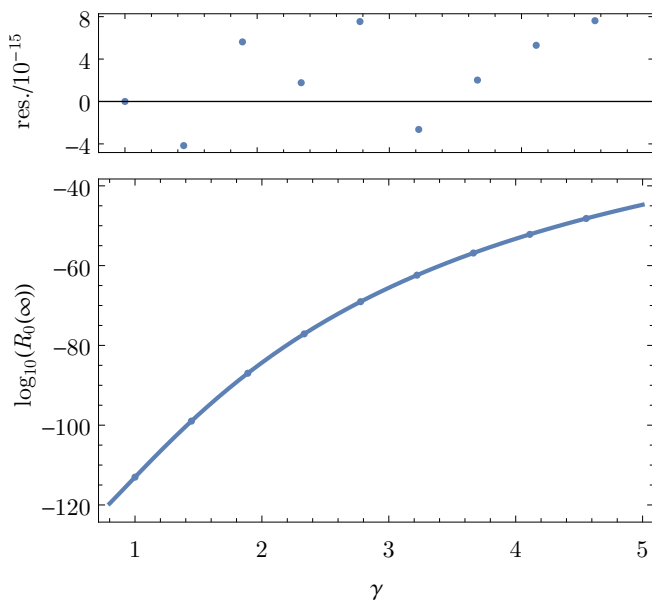


FIG. 5. Comparison of the analytic solution (line) and numerical results (points) of the Riccati equation for a single Sauter pulse with $E = E_S/100$ and $k_3 = 0$. The top plot shows the relative deviation from the analytic result.

as many significant digits in the calculation as needed to give accurate results.

As a benchmark, we calculated $R_{p=0}(\mathcal{T})$ for a single Sauter pulse, which we can again compare to the known

analytical result. Indeed, using very little computational resources [26], it is possible to reproduce the analytic solution for $p = 0$ and various values of γ with a relative error of less than 10^{-14} for a field strength of $E = E_S/100$, see Fig. 5.

V. SUMMARY AND CONCLUSION

Using the worldline instanton method, we have been able to numerically calculate and find analytical approximations for the pair production rate in the dynamically assisted Sauter-Schwinger effect. Building on [6], this now includes the quantum mechanical fluctuation prefactor, which is shown not to counteract the mechanism of dynamical assistance.

Comparing the different pulse shapes considered, they all exhibit a similar qualitative behavior. This includes a region of negligible dependence on the time dependent field up to a threshold value of the Keldysh parameter γ , beyond which the pair production rate is exponentially enhanced.

This threshold γ^{crit} is independent of ε for the Sauter and Lorentzian pulses, in contrast to the sinusoidally varying field and Gaussian pulse which is caused by the different analytic structure of the field profiles.

Furthermore, using a numerical integration of the Riccati equation, we have shown that these results are not an artifact of the semiclassical approximation, but are present in a full numerical simulation as well.

-
- [1] F. Sauter, *Zeitschrift für Phys.* **69**, 742 (1931).
 - [2] F. Sauter, *Zeitschrift für Phys.* **73**, 547 (1932).
 - [3] W. Heisenberg and H. Euler, *Zeitschrift für Phys.* **98**, 714 (1936).
 - [4] J. Schwinger, *Phys. Rev.* **82**, 664 (1951).
 - [5] R. Schützhold, H. Gies, and G. Dunne, *Phys. Rev. Lett.* **101**, 4 (2008), arXiv:arXiv:0807.0754v1.
 - [6] M. F. Linder, C. Schneider, J. Sicking, N. Szpak, and R. Schützhold, *Phys. Rev. D* **085009**, 1 (2015), arXiv:1505.05685.
 - [7] R. Feynman, *Phys. Rev.* **80**, 440 (1950).
 - [8] I. K. Affleck, O. Alvarez, and N. S. Manton, *Nucl. Phys. B* **197**, 509 (1982).
 - [9] C. Schubert, *Phys. Rep.* **355**, 73 (2001).
 - [10] S. P. Kim and D. N. Page, *Phys. Rev. D* **65**, 1 (2002), arXiv:0005078 [hep-th].
 - [11] G. Dunne and C. Schubert, *Phys. Rev. D* **72**, 105004 (2005).
 - [12] G. Dunne, Q.-h. Wang, H. Gies, and C. Schubert, *Phys. Rev. D* **73**, 065028 (2006).
 - [13] C. Schubert, *Sch. Spinn. Part. Quantum F. Theory Worldline Formalism, High. Spins Conform. Geom.* (2012).
 - [14] This does however not mean that the results for 3 + 1-dimensional spacetime are identical, we will highlight the differences in Section II.
 - [15] S. Coleman, *Aspects of Symmetry* (Cambridge University Press, Cambridge, 1985).
 - [16] H. Kleinert, *Path Integrals in Quantum Mechanics, Statistics, Polymer Physics, and Financial Markets*, EBL-Schweitzer (World Scientific, 2009).
 - [17] K. Kirsten and A. J. McKane, *Ann. Phys. (N. Y.)* **308**, 502 (2003), arXiv:0305010 [math-ph].
 - [18] M. Morse, *The Calculus of Variations in the Large*, American Mathematical Society No. Bd. 18 (American mathematical society, 1934).
 - [19] F. Hebenstreit, R. Alkofer, and H. Gies, *Phys. Rev. D* **82**, 105026 (2010).
 - [20] C. Schneider and R. Schützhold, *JHEP* **2016**, 1 (2016), arXiv:arXiv:1407.3584v3.
 - [21] C. K. Dumlu and G. V. Dunne, *Phys. Rev. D - Part. Fields, Gravit. Cosmol.* **83**, 1 (2011), arXiv:1102.2899.
 - [22] M. Orthaber, F. Hebenstreit, and R. Alkofer, *Phys. Lett. B* **698**, 80 (2011).
 - [23] Predictor-Corrector Adams method, default algorithm of Wolfram Mathematica's `NDSolve` function.
 - [24] A. Abad, R. Barrio, F. Blesa, and M. Rodríguez, *ACM Trans. Math. Softw.* **39**, 1 (2012).
 - [25] L. Fousse, G. Hanrot, V. Lefèvre, P. Pélissier, and P. Zimmermann, *ACM Trans. Math. Softw.* **33**, 13 (2007).
 - [26] About one minute per point on a typical desktop PC.